Pergamon

0017-9310(93)E0012-J

Thermocapillary, buoyancy and shear-driven flow within thin annular fluid collars

RUSSELL G. KEANINI

Department of Mechanical Engineering and Engineering Science, University of North Carolina at
Charlotte, Charlotte, NC 28223, U.S.A.

Abstract—A leading order solution for thermocapillary, buoyancy, and shear-driven flow within a thin, fixed-length, annular fluid collar is determined. The solution is based on the assumption that $C/\varepsilon^3 = O(1)$, where C is the capillary number and ε is the collar aspect ratio. In contrast to earlier models of flow within bridges, boundary layer matching near the end regions is not required since end walls are absent. The leading order velocity field is self-similar in the radial direction with the size of the similarity profiles determined by an unspecified surface heat flux distribution, an unspecified surface shear distribution, and by the unknown capillary surface shape. Conditions leading to thermocapillary, buoyant, or shear driven single and multi-cellular flow are identified. The capillary surface shape is determined using a minimization technique, with the object function defined as the difference between known and iteratively calculated collar volumes. The surface and flow solutions are illustrated using an exponentially decaying surface heat flux and a constant external shear.

1. INTRODUCTION

THERMOCAPILLARY and buoyancy driven flow within annular fluid collars arises in a number of circumstances: during drilling of materials by high energy density heat sources, during laser machining of computer chips, during wire coating operations, and during heating or cooling of fluid layers within cylindrical pores, for example. Some applications utilize some form of gas assist in order to increase penetration capabilities or to shield the heat source or material surface from the surrounding atmosphere. The collars may be subject to various combinations of thermocapillary, pressure, external shear, buoyancy, and/or Lorentz forces.

Most of the theoretical studies treating flow within fluid annuli have focused on stability questions [1–4]. Of this work, the last considered thermocapillarity, while the second accounted for surface shear due to a second fluid within the annular core. A number of relevant theoretical studies have dealt with thermocapillary driven flow or instability within liquid bridges (see, e.g. Sen and Davis [5]; Xu and Davis [6, 7]; Rybicki and Florian [8, 9]). Sen and Davis [5] used matched asymptotic expansions to determine the thermocapillary flow and capillary interface shape within a narrow bridge subject to a linearly varying external gas temperature. They considered the case of small bridge aspect ratio, ε, assumed that the Reynolds and Marangoni numbers were each on the order of ε, and based their analysis on the distinguished limit

$C/\varepsilon^4 = O(1)$, where C is the capillary number. Xu and Davis [6], assuming $C/\varepsilon = O(1)$, obtained similarity solutions for the core flow (away from end-walls) within thin, heated, axisymmetric bridges. Since boundary layer flows within the end regions were not determined, order unity Re and Ma could be accommodated. Rybicki and Florian [8] determined flow solutions within liquid bridges having order unity aspect ratios. Their analysis was based on an assumed, physically consistent capillary surface shape and on the assumptions that $Re \to 0$ and $Ma \to 0$.

The objective of the present study is to investigate flow and heat transfer within thin axisymmetric fluid collars subject to thermocapillary, buoyant and external shear forces. While a number of theoretical studies [5, 6, 8] have treated thermocapillary and buoyant flow within liquid bridges, it appears that no equivalent studies have been carried out concerning flow within collars. Since external shear forces are often important in collar flow (in contrast to bridge flow), this feature will be examined as well. Leading order solutions for the two-dimensional velocity and temperature fields are obtained in terms of the unknown capillary surface shape and unspecified external heat flux and shear stress distributions. A minimization technique is developed and tested in order to calculate the capillary surface shape. The model allows examination of a range of flow and heat transfer phenomena associated with various buoyant, thermocapillary, external shear and external heating regimes.

NOMENCLATURE

A geometric parameter, equation (3); also dimensionless area, equation (48)

A_0, A_c exact and candidate surface areas, equation (49)

Br Brinkman number, equation (11)

C capillary number, $\mu W_s/\sigma_o$

$\bar{C}$ constant, equation (26)

$\hat{e}_x, \hat{e}_z$ unit vectors in x and z directions

F object function, equation (37)

G_1, G_2, G_3, G_4 functions comprising U_o, equation (32)

Gr Grashof number, equation (11)

h, H dimensionless capillary surface height

k thermal conductivity

L^* collar length

L dimensionless length, equation (48)

m_0, m_1 capillary surface slopes at endpoints

Ma Marangoni number, equation (11)

$\hat{n}$ unit normal vector, equation (13)

n_i unit normal vector component

P^* pressure

P dimensionless pressure, equation (1); $\Delta P^* R^*/2\sigma$, equation (45)

P_e^* external pressure

P_s pressure scale, equation (5)

Pr Prandtl number, v/α

q^* external heat flux distribution

Q dimensionless external heat flux distribution, $q^*(z^*)\delta_o/(k\Delta T^o)$

r^* radial coordinate

R^* inside radius of cylinder

Re_δ Reynolds number, equation (11)

$\hat{t}$ unit tangent vector, equation (13)

t_i unit tangent vector component

T^* temperature

u^* radial velocity

u_i^* velocity component

U dimensionless radial velocity, equation (1)

U_p wall speed, equation (33a)

V_c dimensionless candidate volume, equation (38)

V_o collar volume

w^* axial velocity

W dimensionless axial velocity, equation (1)

W_s velocity scale, equation (4)

x^* radial coordinate

X dimensionless radial coordinate, equation (1)

z^* axial coordinate

Z dimensionless axial coordinate, equation (1).

Greek symbols

α thermal diffusivity

β coefficient of thermal expansion

γ_T derivative of surface tension coefficient with respect to temperature

δ_{ij} Kronecker delta function

δ_o characteristic collar thickness, equation (2)

ΔT^o characteristic temperature difference, equation (6)

$\varepsilon_1, \varepsilon_2$ collar aspect ratios, equation (3)

ε_c approximated capillary surface heights at endpoints, equation (35a)

ε_v convergence tolerance, equation (41)

η dimensionless radial coordinate, X/h_o

Θ dimensionless temperature, equation (1)

μ dynamic viscosity

v kinematic viscosity

ρ density

σ surface tension coefficient, equation (20)

σ_{ij}^* stress tensor, equation (19)

σ_o surface tension coefficient at reference temperature

$\sigma_{lg}, \sigma_{sg}, \sigma_{sl}$ surface tension coefficients between liquid and gas, solid and gas, and solid and liquid, respectively, equation (40)

Σ dimensionless external shear stress distribution, $\tau\delta_o/(\mu W_s)$

τ external shear stress distribution

χ $[1+(dH/dZ)^2]^{-1/2}$

ψ stream function.

Subscripts

min   minimum

o   zero order.

Superscripts

ex   exact

o,min   initial guess closest to exact value

$*$ dimensional quantity.

2. ANALYSIS

2.1. Scaling

The problem is formulated in cylindrical coordinates and is depicted in Fig. 1. For the present problem, the following non-dimensional quantities are introduced:

$$X = \frac{(R^*-r^*)}{\delta_o}, \quad Z = \frac{z^*}{L^*}, \quad U = \frac{u^*}{\varepsilon_1 W_s},$$
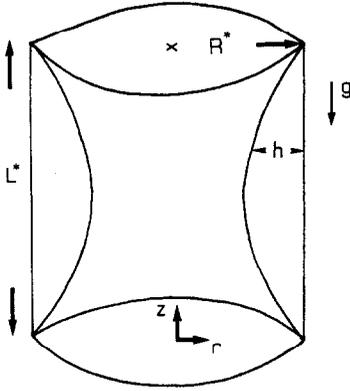
FIG. 1. Schematic of a thin annular fluid collar within a cylinder.

$$W = \frac{w^*}{W_s}, \quad P = \frac{p^* - p_e^*}{P_s}, \quad \Theta = \frac{(T^* - T_o^*)}{(T_m^* - T_o^*)} \quad (1)$$

where R^* is the cylinder's inside radius, L^* is either the cylinder length or the collar wavelength (when a series of collars exist), T_m^* is the maximum fluid temperature, T_o^* is a reference temperature, P_e^* is a constant external pressure, and where the rest of the quantities are defined below. The liquid layer thickness is characterized by δ_o, which will be defined as

$$\delta_o = \frac{V_o}{\pi R^* L^*} \quad (2)$$

where V_o is the total liquid volume. As shown in Fig. 1, gravity acts in the negative z-direction. Three geometric parameters are defined as

$$A = \frac{R^*}{L^*}, \quad \varepsilon_1 = \frac{\delta_o}{R^*}, \quad \varepsilon_2 = \frac{\delta_o}{L^*}. \quad (3)$$

The axial velocity scale W_s follows by balancing viscous shear against thermocapillary stress

$$\frac{\mu W_s}{\delta_o} \sim \frac{\gamma_T \Delta T^o}{L^*}$$

so that

$$W_s = \frac{\gamma_T \Delta T^o \delta_o}{\mu L^*}. \quad (4)$$

We are thus focusing on the viscous flow limit discussed by Ostrach [10]. The radial velocity scale, $\varepsilon_2 W_s$, is a consequence of the continuity equation while the pressure scale is the lubrication pressure scale

$$P_s = \frac{\mu W_s}{\varepsilon_2 \delta_o}. \quad (5)$$

The temperature scale is defined as the difference between the maximum liquid temperature and the reference temperature:

$$\Delta T^o = T_m^* - T_o^*. \quad (6)$$

2.2. Governing equations

Introducing the above non-dimensional variables and parameters into the continuity, momentum, and energy equations and utilizing the Bousinesq approximation, we obtain the following:

Continuity

$$U_X + W_Z = \varepsilon_1(1 + \varepsilon_1 X)U + O(\varepsilon_1^3) \quad (7)$$

X-momentum

$$P_X = -\varepsilon_2^3 Re_\delta[UU_X + WU_Z] + \varepsilon_2^3 U_{XX} + O(\varepsilon_2^2 \varepsilon_1) \quad (8)$$

Z-momentum

$$W_{XX} + \frac{Gr}{Re_\delta}\Theta - P_Z = \varepsilon_2 Re_\delta[UW_X + WW_Z]$$
$$+ \varepsilon_1 W_X - \varepsilon_2^2 W_{ZZ} + \varepsilon_1^2 X W_X + O(\varepsilon_1^3) \quad (9)$$

Energy

$$\Theta_{XX} = \varepsilon_2 Ma[U\Theta_X + W\Theta_Z] + \varepsilon_1 \Theta_X + \varepsilon_1^2 X \Theta_X$$
$$- \varepsilon_2^2 \Theta_{ZZ} - Br W_X^2 + O(\varepsilon_2 Br). \quad (10)$$

First and second partial derivatives of U, W, P, and Θ with respect to X and Z are denoted by subscripts and r^{*-1} has been expanded as $R^{*-1}(1 + \varepsilon_1 X + \varepsilon_1^2 X^2 \cdots)$. The Reynolds, Grashof, Marangoni and Brinkman numbers are defined as

$$Re_\delta = \frac{W_s \delta_o}{\nu}, \quad Gr = \frac{g\beta\Delta T^o \delta_o^3}{\nu^2},$$
$$Ma = Pr Re_\delta = \frac{W_s \delta_o}{\alpha}, \quad Br = \frac{\mu W_s^2}{k\Delta T^o} \quad (11)$$

where $Pr = \nu/\alpha$ is the Prandtl number. Equations (7)–(9) are similar to equations derived for thermocapillary and buoyancy-driven flow in a rectangular cavity [10], and with the exception of terms multiplying $1/r^*$, have the same ordering in ε_2, and in products of ε_2 and Ma and ε_2 and Re_δ as those derived by Sen and Davis [5].

2.3. Boundary conditions

The unknown capillary surface is defined as

$$X = h(Z), \quad 0 \leqslant Z \leqslant 1. \quad (12)$$

The corresponding unit normal and tangent vectors are

$$\hat{n} = (\hat{e}_x - \varepsilon_2 h' \hat{e}_z)/N, \quad \hat{t} = (\hat{e}_z + \varepsilon_2 h' \hat{e}_x)/N \quad (13)$$

where $N = (1 + \varepsilon_2^2 h'^2)^{1/2}$ and $h' = dh/dZ$. The normal and tangential stress boundary conditions on h are given by

$$\sigma_{ij}^* n_i n_j = -\sigma n_{i,i} \quad (14)$$

and

$$\sigma_{ij}^* t_i n_j = -\gamma_T T_{,i}^* t_i - \tau \quad (15)$$

where $\tau = \tau(z^*)$ is an unspecified external shear stress. The thermal boundary condition and no-penetration condition on h are given by

$$kT_{,i}^* n_i = q^* \quad (16)$$

and

$$u^*_{i,j}n_j = 0 \qquad (17)$$

where $q^* = q^*(z^*)$ is an unspecified surface heat flux. Along the cylinder wall, no-slip and isothermal wall conditions are imposed:

$$u^* = w^* = 0, \quad T^* = T^*_0, \quad r^* = R^*, \quad 0 \leqslant z^* \leqslant L^*. \qquad (18)$$

Flux or non-isothermal conditions can be readily imposed along the wall, depending on the circumstances. The stress tensor is given as

$$\sigma^*_{ij} = -P^*\delta_{ij} + \mu(u^*_{i,j} + u^*_{j,i}) \qquad (19)$$

and a linear equation of state is assumed for the surface tension

$$\sigma = \sigma_0 - \gamma_T(T^* - T^*_0) \qquad (20)$$

where γ_T is the temperature derivative of the surface tension, and where σ_0 is the surface tension magnitude at T^*_0.

Following non-dimensionalization, the normal and tangential boundary conditions on h become:

$$P = \varepsilon_2\left(\frac{\varepsilon_2}{C} - \Theta\right)[A^{-1} + \varepsilon_2 A^{-2}h + \varepsilon_2 h''] + O\left(\frac{\varepsilon_2^4}{C}\right) \qquad (21)$$

$$W_X + \Theta_X h' + \Theta_Z = -\Sigma + O(\varepsilon_2^2) \qquad (22)$$

where $C = \mu W_s/\sigma_0$ is the capillary number and $\Sigma = \tau\delta_0/(\mu W_s)$ is the non-dimensional shear stress. The thermal boundary condition and no-penetration condition on h are given by

$$\Theta_X = Q + O(\varepsilon_2^2) \qquad (23)$$

and

$$U - Wh' = 0 \qquad (24)$$

where $Q = q(z^*)\delta_0/(k\Delta T^0)$. Along the cylinder wall,

$$U(0, Z) = W(0, Z) = \Theta(0, Z) = 0, \quad 0 \leqslant Z \leqslant 1. \qquad (25)$$

End conditions on h are discussed in Section 2.8.

2.4. Leading order solution for $\varepsilon_2 \to 0$, $Re_\delta = o(\varepsilon_2^{-1})$, $Ma = o(\varepsilon_2^{-1})$, $Br \to 0$

We seek a solution for the case where $\varepsilon_2 \to 0$, $Re_\delta = o(\varepsilon_2^{-1})$, $Ma = o(\varepsilon_2^{-1})$, and $Br \to 0$. The present conditions are similar to those introduced by Xu and Davis [6] and are less restrictive than those used by Sen and Davis [5] and Rybicki and Florian [8] (i.e. $Re \to 0$, $Ma \to 0$, and in the latter case, $Br = 0$). The assumption that Br is small means that viscous dissipation is negligible. Rayleigh's stability criterion for (isothermal) annular films within cylinders suggests that A should be greater than approximately $1/2\pi$ (see below).

A self-consistent solution results if

$$C = \bar{C}\varepsilon_2^3 \qquad (26)$$

where $\bar{C} = O(1)$. This distinguished limit is slightly less restrictive than the limit $C/\varepsilon^4 = O(1)$, introduced

by Sen and Davis [5] and more restrictive than the $C/\varepsilon = O(1)$ limit used by Xu and Davis [6]. Since end walls are not present, however, the present limit allows whole-field solutions without the need for boundary layer matching [5]. We assume solutions of the form

$$P = \varepsilon_2^{-1}P_{-1} + P_0 + \varepsilon_1 P_{10} + \varepsilon_2 P_{01} + \cdots \qquad (27a)$$

$$\{U, W, \Theta, h\} = \{U_0, W_0, \Theta_0, h_0\}$$
$$+ \varepsilon_1\{U_{10}, W_{10}, \Theta_{10}, h_{10}\}$$
$$+ \varepsilon_2\{U_{01}, W_{01}, \Theta_{01}, h_{01}\} + \cdots. \qquad (27b)$$

The first term in P provides the static pressure induced by mean surface tension. In particular, the lowest order problem

$$P_{-1,Z} = P_{-1,X} = 0, \quad P_{-1} = (\bar{C}A)^{-1} \qquad (28)$$

leads directly to

$$P^* - P^*_e = \frac{\sigma_0}{R^*}.$$

It is important to note that the lowest order (i.e. static pressure) term in P is independent of the assumption in (26). This is perhaps most easily seen by redefining P in (21) as $P - \bar{P}$, where $\bar{P} (= (AC)^{-1}\varepsilon_2^2)$ is the non-dimensional equivalent of the last equation. Note that Rybicki and Florian [8] utilized a similar pressure expansion in their treatment of flow within bridges.

At the next order, we have the following.

$$W_{0,XX} + \frac{Gr}{Re_\delta}\Theta_0 - P_{0,Z} = 0 \qquad (28a)$$

$$U_{0,X} + W_{0,Z} = 0 \qquad (28b)$$

$$P_{0,X} = 0 \qquad (28c)$$

$$\Theta_{0,XX} = 0 \qquad (28d)$$

$$P_0 = \bar{C}^{-1}(h''_0 + A^{-2}h_0) \qquad (28e)$$

$$W(0, Z) = U(0, Z) = \Theta(0, Z) = 0 \qquad (28f,g,h)$$

$$W_{0,X} + \Theta_{0,X}h'_0 + \Theta_{0,Z} + \Sigma = 0 \quad \text{on} \quad X = h_0 \qquad (28i)$$

$$U_0 - W_0 h'_0 = 0 \quad \text{on} \quad X = h_0 \qquad (28j)$$

$$\Theta_{0,X} = Q \quad \text{on} \quad X = h_0. \qquad (28k)$$

2.5. Leading order solution

Conditions (28h) and (28k) are used to solve the energy equation (28d). The solution is

$$\Theta_0(\eta, Z) = Q(Z)h_0\eta \qquad (29)$$

where $\eta = X/h_0$. Eliminating pressure between the Z- and X-momentum equations (28a) and (28c), using (29), introducing (28i), and using the relationship

$$W_0 h'_0 - U_0 = \frac{\partial}{\partial Z}\int_0^{h_0(Z)} W_0\,dX = 0 \qquad (30)$$

we arrive at the solution for W_0

$$W_o(\eta, Z) = \frac{Gr}{Re_\delta} Q h_o^3 \left(-\frac{\eta^3}{6} + \frac{5}{16}\eta^2 - \frac{1}{8}\eta \right)$$

$$+ \left(\Sigma + \frac{d(h_o Q)}{dZ} \right) h_o \left(-\frac{3}{4}\eta^2 + \frac{1}{2}\eta \right). \quad (31)$$

Introducing (31) into the continuity equation, (28b), and imposing condition (28g), we obtain the solution for U_o

$$U_o(\eta, Z) = G_1 + G_2 + G_3 + G_4 \quad (32)$$

where

$$G_1 = \frac{Gr}{Re_\delta} \frac{dQ}{dZ} h_o^4 \left(\frac{\eta^4}{24} - \frac{5}{48}\eta^3 + \frac{\eta^2}{16} \right)$$

$$G_2 = -\frac{Gr}{Re_\delta} Q \frac{dh_o}{dZ} h_o^3 \left(\frac{5}{48}\eta^3 - \frac{1}{8}\eta^2 \right)$$

$$G_3 = \frac{1}{4} \left(\frac{d\Sigma}{dZ} + \frac{d^2(Qh_o)}{dZ^2} \right) h_o^2 (\eta^3 - \eta^2)$$

$$G_4 = -\frac{1}{4} \left(\Sigma + \frac{d(Qh_o)}{dZ} \right) h_o \frac{dh_o}{dZ} \eta^3.$$

Equations (31) and (32) are similarity solutions in the normalized radial coordinate η. Xu and Davis [6] also obtained similarity solutions in their treatment of flow within liquid bridges. It is important to note however, that since $h_o(0) = h_o(1) = 0$, then to first order, zero velocity conditions hold at the end points. Thus, at leading order, boundary layer matching is not necessary. Note, if $\gamma_T > 0$ (corresponding to thermocapillary stresses acting from cool to warm regions), then each coefficient of $(Qh_o)'$ and $(Qh_o)''$ in (31) and (32) must be multiplied by -1.

2.6. Characteristics of leading order solution

The leading order velocity solution in (31) and (32) encompasses a wide range of possible flow regimes. For example, in the limit $|(GrQ/Re_\delta)/(\Sigma + (Qh_o)')| \to 0$, the flow is determined by thermocapillary and/or external shear stresses. In this limit, either multi-cell or single-cell flow can arise, depending on how $(\Sigma + (h_o Q)')$ varies with Z. In multi-cell flow, $(\Sigma + (h_o Q)') = 0$ at n points $Z_1, Z_2, \ldots, Z_n$ on $0 \leqslant Z \leqslant 1$. In this case, $n+1$ counter-rotating cells (toroidal vortices) appear, each separated by horizontal stagnation streamlines lying on $Z = Z_1 - Z_n$. In particular, since $W_o \sim (\Sigma + (h_o Q)') h_o(-3/4\eta^2 - \eta/2)$, then at each Z_i, $W_o(h_o, Z_i) \sim 0$. From the kinematic condition (24), $U_o(h_o, Z_i)$ also equals zero. Thus, from the stream function corresponding to W_o and U_o,

$$\psi = \frac{Gr}{8Re_\delta} Q h_o^4 \left(-\frac{\eta^4}{3} + \frac{5}{6}\eta^3 - \frac{\eta^2}{2} \right)$$

$$+ \frac{1}{4} (\Sigma + (h_o Q)') h_o^2 (\eta^2 - \eta^3) \quad (32a)$$

it is apparent that the corresponding stagnation

streamlines are horizontal. It should be noted that when $\Sigma = 0$, the dividing streamlines coincide with critical points in the surface temperature distribution, $\Theta_o h_o$. Note too that in this latter case the direction of rotation in each vortex is reversed if $\gamma_T > 0$ (refer to Section 2.5).

Single-cell flow in the limit $|(GrQ/Re_\delta)/(\Sigma + (Qh_o)')| \to 0$, arises if $(\Sigma + (h_o Q)') \neq 0$ on $0 \leqslant Z \leqslant 1$. In this case, the flow is dominated by a single vortex with the direction of rotation determined by the sign of $(\Sigma + (h_o Q)')$. In both single-cell and multi-cell flows, W_o is parabolic in η (within any given cell), having a vertex at $\eta = 1/3$, passing through zero at $\eta = 2/3$, and reaching its maximum magnitude at the capillary surface.

In the limit $|(\Sigma + (Qh_o)')/(GrQ/Re_\delta)| \to 0$, the flow is buoyancy dominated. Similar to the limit of shear-driven flow, single- or multi-cell flow can arise depending on the behavior of $Q(Z)$. Multiple cells occur if $Q = 0$ on $0 \leqslant Z \leqslant 1$ (again separated by horizontal streamlines), while single cells arise if $Q \neq 0$. In any given cell, W_o is cubic in η, having a vertex at $\eta = 1/4$, a zero crossing at $\eta = (15 - \sqrt{33})/16$, and a maximum magnitude at the surface. On heated intervals ($Q > 0$), W_o is negative at $\eta = 1/4$ and positive at the surface, with the signs changing on cooled intervals. In this limit it is interesting to note that buoyant effects in microgravity can be damped (amplified) by use of a small (large) axially uniform heat source.

The leading order temperature solution in equation (29) corresponds to the conduction limit. Interestingly, the collar's thinness prevents fluid motion from playing a role in leading order heat transfer, even though Re_δ and/or Ma may be large (but not so large that εRe_δ or $\varepsilon Ma = O(1)$; see equations (9) and (10)). Since the leading order temperature varies linearly across the collar, heat flux is purely radial so that the wall flux at any Z is equal to the corresponding flux across the capillary surface.

2.7. Comparison with solution for buoyant flow within a driven slot

We demonstrate the consistency of the preceding formulation by comparing the solution with a similar solution obtained by Arpaci and Larsen [11]. They solved the problem of buoyant Couette–Poiseuille flow and heat transfer within a wall-driven, differentially heated, infinitely long vertical slot. The zero-order governing equations, (28a)–(28d), are identical to those given explicitly and implicitly by Arpaci and Larsen [11]. We recover their problem and solution by first replacing the boundary conditions given by equations (28i) and (28k) with the conditions

$$W_o(h_o, Z) = -U_p, \quad \Theta_o(h_o, Z) = \Theta_2 \quad (33a)$$

(where $\Theta_2 > 0$), then by noting that the normal stress boundary condition (28e) does not apply, and finally by setting h_o equal to a constant. The resulting solution is given as

$$\Theta_o = \Theta_2 \eta \qquad (33b)$$

$$U_o = 0 \qquad (33c)$$

and

$$W_o = -12\Theta_2 h_o^2 \frac{Gr}{Re_\delta}[2\eta^3 - 3\eta^2 + \eta] + U_p[-3\eta^2 + 2\eta] \qquad (33d)$$

where again $\eta = X/h_o$. This is identical (in non-dimensional form) to Arpaci and Larsen's solution (in the case where their cool wall temperature is set equal to the reference temperature). As shown in the earlier work, the first term in equation (33d) provides the velocity induced by buoyancy while the second term gives the velocity induced by external shear.

Comparing the solution in equation (33d) with that in equation (31), we find that for buoyancy dominated flow, W_o changes sign at $\eta = 0.5$ and $\eta = 0.58$ within the vertical slot and fluid collar, respectively. For shear-driven flow, the sign changes occur at $\eta = 2/3$ in both cases.

2.8. Capillary surface solution

The zero-order velocity field can be determined once the surface shape is known. The governing equation for the surface shape follows by differentiating the normal stress equation, (28e), and then by using the solutions for W_o and Θ_o in the Z-momentum equation, (28a). The result is

$$\frac{d^3 h_o}{dZ^3} + \frac{1}{A^2}\frac{dh_o}{dZ} - \frac{5}{8}\frac{Gr\bar{C}}{Re_\delta}Qh_o$$

$$+ \frac{3\bar{C}}{2h_o}\left(\Sigma + \frac{d(Qh_o)}{dZ}\right) = 0. \qquad (34)$$

We will focus on the case of a partially wetting collar within a cylinder of length L^*. The corresponding boundary conditions and volume constraint are:

$$h_o(0) = h_o(1) = 0 \qquad (35)$$

and

$$\int_0^1 h_o \, dZ = \tfrac{1}{2} \qquad (36)$$

where equation (36) is correct to $O(\varepsilon_2)$ and where the $1/2$ follows from equation (2). Note that integrating equation (28a) in order to obtain P_o for use in equation (28e) is argued against since this leads to an integral equation in h_o.

In order to solve equation (34), we utilize a minimization technique in combination with a shooting method. In particular, we define an object function, F, as

$$F = \frac{[(V_c - V_o)^2]^{1/2}}{V_o} \qquad (37)$$

where V_c is a candidate volume

$$V_c = \int_0^1 h_o \, dZ. \qquad (38)$$

Since two of the three boundary conditions on equation (34) are known (conditions (35)), and since a volume constraint must be met, V_c and thus F can be considered a function of one of the two unknown contact angles

$$m_0 = \frac{dh_o(0)}{dZ} \quad \text{or} \quad m_1 = \frac{dh_o(1)}{dZ}.$$

We will assume that

$$F = F(m_1) \qquad (39)$$

although the results discussed below were found to be independent of whether $F = F(m_1)$ or $F = F(m_0)$.

The solution algorithm is as follows.

(1) Initially, two guesses are made for m_1. Subsequent values of m_1 are determined by the simplex algorithm (see, e.g. Spendly et al. [12]; Press et al. [13]).

(2) In order to treat the singular points $Z = 0$ and 1 in equation (34), we use a shooting method and integrate away from the end points to a fitting point ($Z = 0.5$). Since the fluid is partially wetting ($m_1 \neq 0$, $m_2 \neq 0$), we approximate the boundary conditions in equation (35) with

$$h_o(0) = h_o(1) = \varepsilon_c \qquad (35a)$$

where $\varepsilon_c = 10^{-4}$ for all calculations. Assuming no fluid film adjacent to the contact lines, Young's equation applies at the endpoints:

$$\frac{dh}{dZ} = \varepsilon_2^{-1}\left(\left(\frac{\sigma_{lg}}{\sigma_{sg} - \sigma_{sl}}\right)^2 - 1\right)^{1/2}, \quad Z = 0, 1 \qquad (40)$$

where σ_{lg}, σ_{sg} and σ_{sl} are the surface tension coefficients between the liquid and gas, solid and gas, and solid and liquid, respectively. By Taylor expanding h_o and using (40), or by introducing the strained coordinate $\zeta = Z/\varepsilon$ (or $\zeta - (Z-1)/\varepsilon$ for $Z \to 1$) into equation (34), it is seen that $h_o \sim Z$ (or $h_o \sim 1 - Z$) near the end points. Thus, for partially wetting fluids integration of equation (34) can begin at Z values near 0 and 1, or equivalently by use of the approximate conditions given in equation (35a). Each updated value of m_1 is used along with the conditions in equation (35a) to integrate equation (34).

(3) The resulting surface solution allows calculation of V_c based on equation (38).

(4) If a convergence criterion

$$F \leqslant \varepsilon_v (= 10^{-4}) \qquad (41)$$

is satisfied, then the corresponding surface solution is used to calculate the velocity field. Otherwise, the simplex algorithm adjusts m_1 and the program returns to step 2. Corriel et al. [14] used a similar approach, based on Newton–Raphson iteration, in their solution of static capillary surfaces.

The program was tested against two known solu-

tions: (1) the exact solution of equation (34) in the case where $A = 1$; $Gr/Re_\delta = Q = \Sigma = 0$, and (2) the solution of the Young–Laplace equation in the case of zero interfacial pressure jump (cycloid solution). The simplex algorithm requires two initial guesses for m_1 and the success of the procedure is largely determined by how close the guesses are to the actual value, m_1^{ex}. In the first test case, the exact solution to equation (34), subject to the given simplifications is

$$h_o(Z) = 5.399 \, (\tan (0.5) \sin (Z) + \cos (Z) - 1). \quad (42)$$

Denoting $m_1^{o,min}$ as the initial guess in closest proximity to m_1^{ex}, it was found that accurate solutions, defined by the condition

$$\max \left(|h_o^{exact} - h_o|/h_o^{exact} \right) < 10^{-2} \quad (43)$$

(evaluated at 8000 positions between the end points) could be obtained for

$$|m_1^{o,min} - m_1^{ex}| < \sim 300 \quad (44)$$

(where $m_1^{ex} = -2.950$). Thus, the minimization program proved very robust in this case.

In the second test case, the Young–Laplace equation can be written as

$$\chi^3 \frac{d^2 H}{dZ^2} - \frac{\chi}{H} = P \quad (45)$$

where $H = h^*/R^*$, $P = \Delta P^* R^*/2\sigma$, and $\chi = [1 + (dH/dZ)^2]^{-1/2}$. In the case of zero interfacial pressure jump, the solution of equation (45) is a catenoid:

$$H = H_o \cosh \left(\frac{Z}{H_o} \right) \quad (46)$$

where

$$H(0) = H_o, \quad H(L) = 1.$$

In order to test the program against this solution, we rearrange and then differentiate equation (45) to arrive at a third order equation in H:

$$H''' - 2 \frac{H'H''}{H} + (1 + (H')^2) \frac{H'}{H^2} = 0. \quad (47)$$

The solution (46) can describe the shape of an annular film suspended between two circular rings (of radius R^*). In this case, solutions have to satisfy an area constraint

$$A = 2\pi \int_0^L H(1 + H_x^2)^{1/2} \, dx \quad (48)$$

so that an appropriate object function is

$$F = \frac{((A_c - A_o)^2)^{1/2}}{A_o} \quad (49)$$

where

$$A_o = 2\pi H_o [L/H_o + \tfrac{1}{2} \sinh (2L/H_o)].$$

For H_o arbitrarily set equal to 0.5 ($L = 0.5 \cosh^{-1}$ (2)), solutions satisfying equation (43) followed for

$$|m_1^{o,min} - m_1^{ex}| < \sim 1.3 \quad (50)$$

where $m_1^{ex} = H(L) = 1.732$.

The program failed to converge to a minimum in F, i.e. failed to satisfy condition (41), for initial guesses lying outside the approximate ranges given in equations (44) and (50). Thus, every test run leading to a minimum in F also satisfied equation (43). Generally, equation (43) was well satisfied, with relative differences between calculated and exact solutions being on the order of 10^{-3}–10^{-5} over approximately 90% of the intervals $0 \leqslant Z \leqslant 1$ (first case) and $0 \leqslant Z \leqslant L$ (second case). As would be expected, the relative accuracy of the solutions increased with decreasing ε_v.

3. RESULTS AND DISCUSSION

3.1. Example: exponentially decaying heat source

The solution given in equations (31)–(32) is stated in terms of two unspecified functions, the surface heat flux, $Q(Z)$, and the external shear distribution, $\Sigma(Z)$. We will specify that

$$Q(Z) = Q_0 \exp [c(Z-1)], \quad \Sigma(Z) = \Sigma_0 \quad (51)$$

where Q_0 and Σ_0 are constants. An exponentially decaying heat flux allows examination of flow and heat transfer behavior ranging from that induced by an approximately constant heat flux ($c \to 0$) to that produced by a strongly decaying flux. The constant stress assumption is satisfied when $(Re_g A)^{-1/2} \ll 1$, where $Re_g (= U_\infty R^*/v_g)$ is the external flow Reynolds number and $A = R^*/L^*$. The velocity and temperature solutions in equations (29), (31) and (32) are fairly general so that a range of external flow and heat transfer conditions can be accommodated.

For the present example, we arbitrarily define the reference flow as the one corresponding to $\bar{C} = 1$, $c = 0.1$, $Q_0 = 0.01$, $Gr/Re_\delta = 1$, $A = 1$, and $\Sigma = 0$. Solutions of equation (34) were obtained for $0 \leqslant Gr/Re_\delta \leqslant 10^4$ ($\gamma_T < 0$), $0 \leqslant c \leqslant 100$, $0 \leqslant \bar{C} \leqslant 1$, $0 \leqslant Q_0 \leqslant 1$, $0 \leqslant \Sigma \leqslant 1$. Referring to Fig. 2(b), we see that the reference flow is dominated by thermocapillarity. Since $(h_o Q')/(Gr/Re_\delta)Q = h_o' + 0.1 h_o$ however, buoyancy will be important where $h_o' \ll 1$. The effect of increasing buoyancy is shown in Fig. 2, where Fig. 2(b) depicts the reference flow, and Figs. 2(c)–(f) correspond to $Gr/Re_\delta = 10$, 100, 1000, and 10000, respectively. Figure 3 shows a similar progression of Gr/Re_δ in the case of positive γ_T. The flows in Figs. 2(b) and 3(b) are thermocapillary-driven, with the flow direction within each counter-rotating cell determined by the sign of γ_T. Since the surface stagnation point occurs where $(h_o Q)' = Gr Q h_o^2/12 Re\delta$ (refer to equation (31)), then for $Gr/Re_\delta \sim 1$ and $Q_o = 0.01$, the stagnation streamlines approach the point of maximum surface temperature. When Gr/Re_δ increases to 10 (Figs. 2(c), 3(c)), one cell becomes larger than the other, with the larger cell produced by
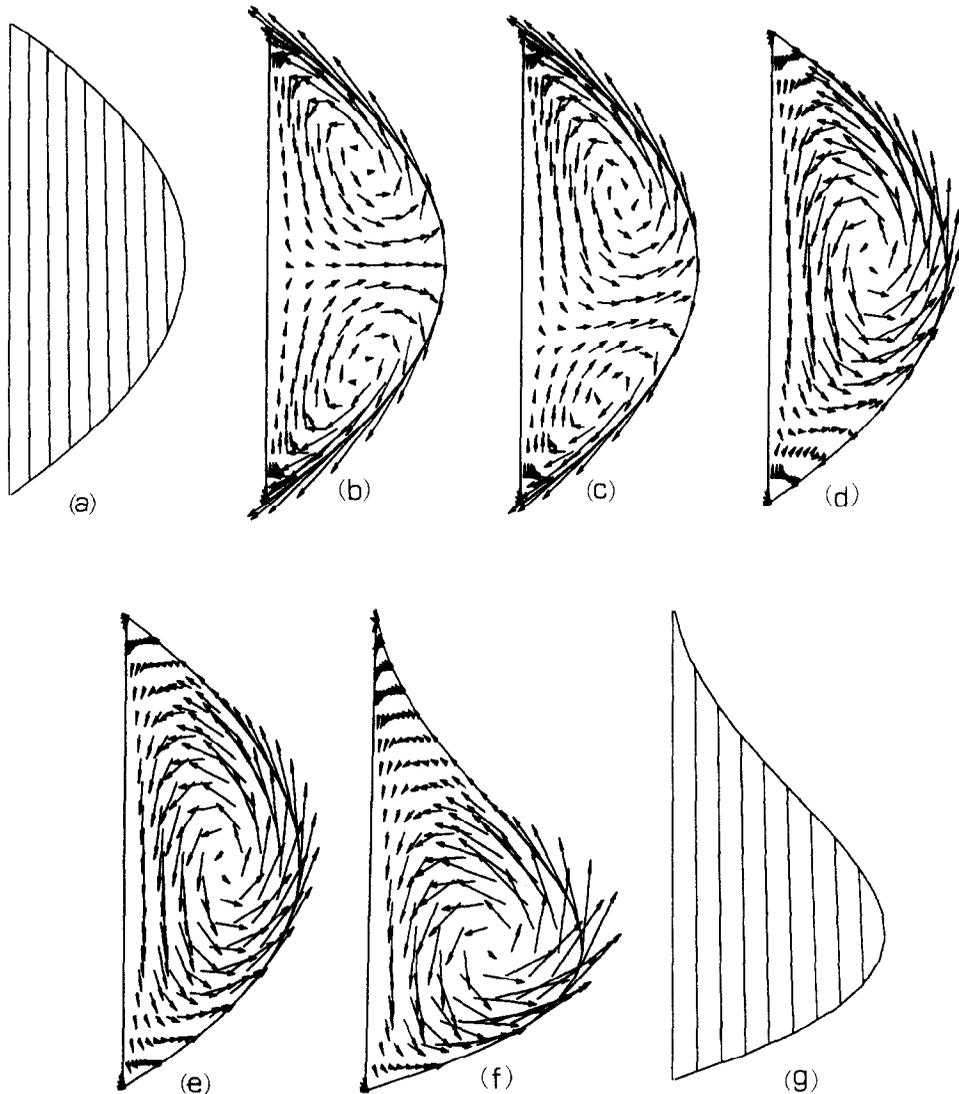
FIG. 2. Effect of Gr/Re_δ. $\bar{C} = 1$, $c = 0.1$, $Q_o = 0.01$, $\Sigma = 0$, $\gamma_T < 0$. (a) Isotherms for $Gr/Re_\delta = 1$. Velocity fields for: (b) $Gr/Re_\delta = 1$, (c) $Gr/Re_\delta = 10$, (d) $Gr/Re_\delta = 100$, (e) $Gr/Re_\delta = 1000$, and (f) $Gr/Re_\delta = 10\,000$. (g) Isotherms for $Gr/Re_\delta = 10\,000$. Isotherms corresponding to cases (c)–(e) are similar to (a).

complementary action of thermocapillarity and buoyancy. Similarly, the small cells occur in the regions where buoyancy and thermocapillarity are in competition. When $Gr/Re_\delta = 100$, the flow is buoyancy dominated. Note, however, that the stagnation point condition $((h_oQ)' = GrQh_o^2/12Re_\delta)$, is still satisfied, as evidenced by the small vortices in the upper ($\gamma_T > 0$) and lower corners ($\gamma_T < 0$). At $Gr/Re_\delta = 1000$, thermocapillary-driven vortices are almost completely suppressed, with the slight bulge within the collar becoming pronounced when Gr/Re_δ reaches $10\,000$ (Fig. 2(f)). Since $Gr/Re_\delta = \rho g\beta\delta_o L^*/\gamma_T$ then the bulging that occurs at large Gr/Re_δ could be associated with increasing collar thickness or length, or with decreases in γ_T due to surfactants, for example. Clearly, the progression of shapes in Fig. 2 could also be associated with changes in gravity. Note that

convergent solutions could not be obtained in the case of $Gr/Re_\delta = 10\,000$, and $\gamma_T > 0$.

The effects of decay rate on the reference flow are shown in Fig. 4. As c increases, the point of maximum surface temperature shifts upward toward $Z = 1$ while the maximum temperature decreases. At any given Z, Q decreases with increasing c so that for approximately fixed wall-to-surface distance and fixed wall temperature, the corresponding surface temperture must also decrease (since Θ_o corresponds to the conduction limit). When $c = 0.1$, the isotherms are essentially parallel to the isothermal wall. However, when $c = 10$, heat transfer is concentrated within the upper portion of the collar with the lower half of the collar remaining essentially isothermal. Since the flow is thermocapillary-driven ($|GrQ/Re_\delta/(h_oQ)'| \ll 1$), the horizontal stagnation streamline separating the upper
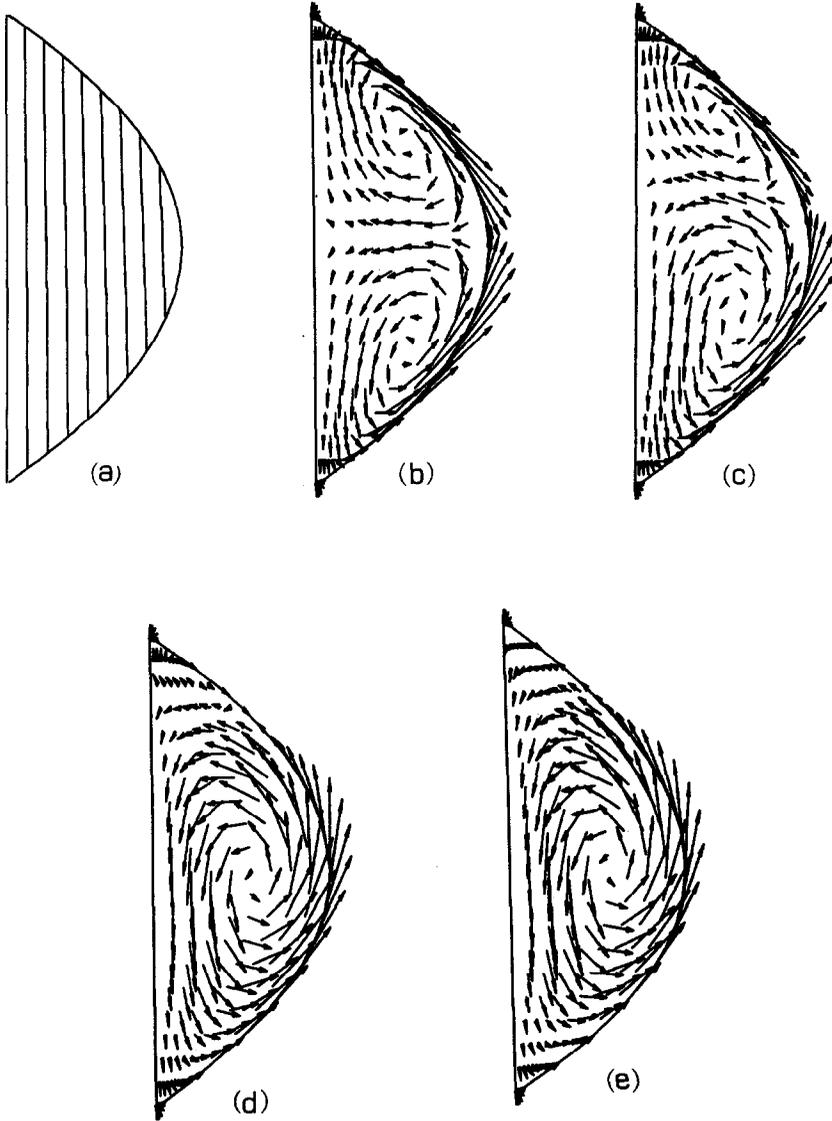
FIG. 3. Effect of Gr/Re_δ. $\bar{C} = 1$, $c = 0.1$, $Q_o = 0.01$, $\Sigma = 0$, $\gamma_T > 0$. (a) Isotherms for $Gr/Re_\delta = 1$. Velocity fields for: (b) $Gr/Re_\delta = 1$, (c) $Gr/Re_\delta = 10$, (d) $Gr/Re_\delta = 100$, and (e) $Gr/Re_\delta = 1000$. Isotherms corresponding to cases (c)–(e) are similar to (a).

and lower cells moves upward with the maximum surface temperature. Due to steepening surface temperature gradients with increasing c, maximum flow speeds, located on the surface, increase with decay rate. Similar results, with the exception that flow directions reverse, follow when $\gamma_T > 0$ (results not shown).

The effect of surface shear stress, Σ, on the reference flow is shown in Fig. 5. As Σ increases from 0.001 to 0.01, thermocapillary flow gives way to shear-driven flow. For $\Sigma = 0.001$ and 0.01, the stagnation point condition, $(\Sigma + (h_o Q)') = GrQh_o^2/12Re_\delta$, can be satisfied, while the flow becomes uni-cellular and shear-driven for $\Sigma = 0.1$ and 1. Again, since $|(GrQ/Re_\delta)/(\Sigma + (h_o Q)')|$ is small, the cells (when $\Sigma = 0.001, 0.01$) are separated by horizontal stagnation streamlines. Figure 6 shows the effect of increasing buoyancy when

$\Sigma = 0.1$. For $Ge/Re_\delta = 1$ and 10, the flow is shear-driven. However, when Gr/Re_δ reaches 100, buoyancy becomes prominent, and a counter-clockwise vortex appears near the wall. Although not resolved in the streamline plot, two clockwise-rotating vortices are apparent in the vector plot, located above and below the wall vortex. Finally, at $Gr/Re_\delta = 1000$, the flow is buoyancy-dominated with the effects of external shear apparent only in the corners.

As discussed in Section 2.6, multi-cellular *buoyancy* driven flow in the limit $|(\Sigma + (Qh_o)')/(GrQ/Re_\delta)| \to 0$, arises if Q changes sign (say at $Z = Z_i$) anywhere along the capillary surface. In this case, by inspection of equation (32a), neighboring cells rotate in opposite directions due to the sign change in Q. Moreover, since W_o and $U_o \sim 0$ at the point $(h_o(Z_i), Z_i)$ (equations (31) and (32)), and since $W_o \sim 0$ along the line $Z = Z_i$,
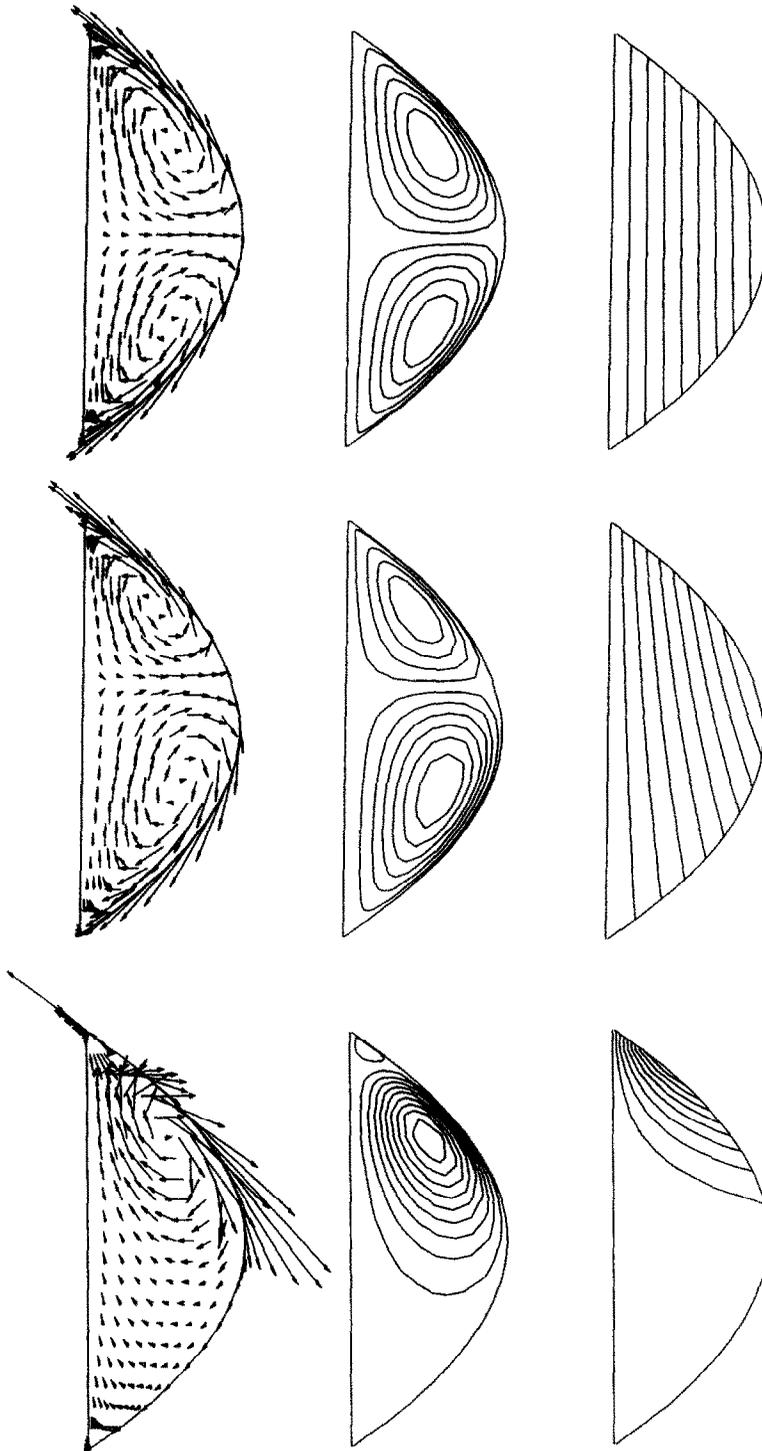
FIG. 4. Effect of decay rate c. $Gr/Re_\delta = 1$, $\bar{C} = 1$, $c = 0.1$, $Q_o = 0.01$, $\Sigma = 0$, $\gamma_T < 0$. First row, showing (left to right) flow field, streamlines, and isotherms, corresponds to $c = 0.1$. Second row corresponds to $c = 1$. Third row corresponds to $c = 10$.

then each counter-rotating cell pair is divided by an essentially horizontal stagnation streamline (lying on Z_i). Thus, multi-cellular thermocapillary and buoyant flow can display very similar characteristics even though fundamentally different driving forces (surface versus volume) operate in each case. The criteria discussed above can be used to differentiate between these limits.
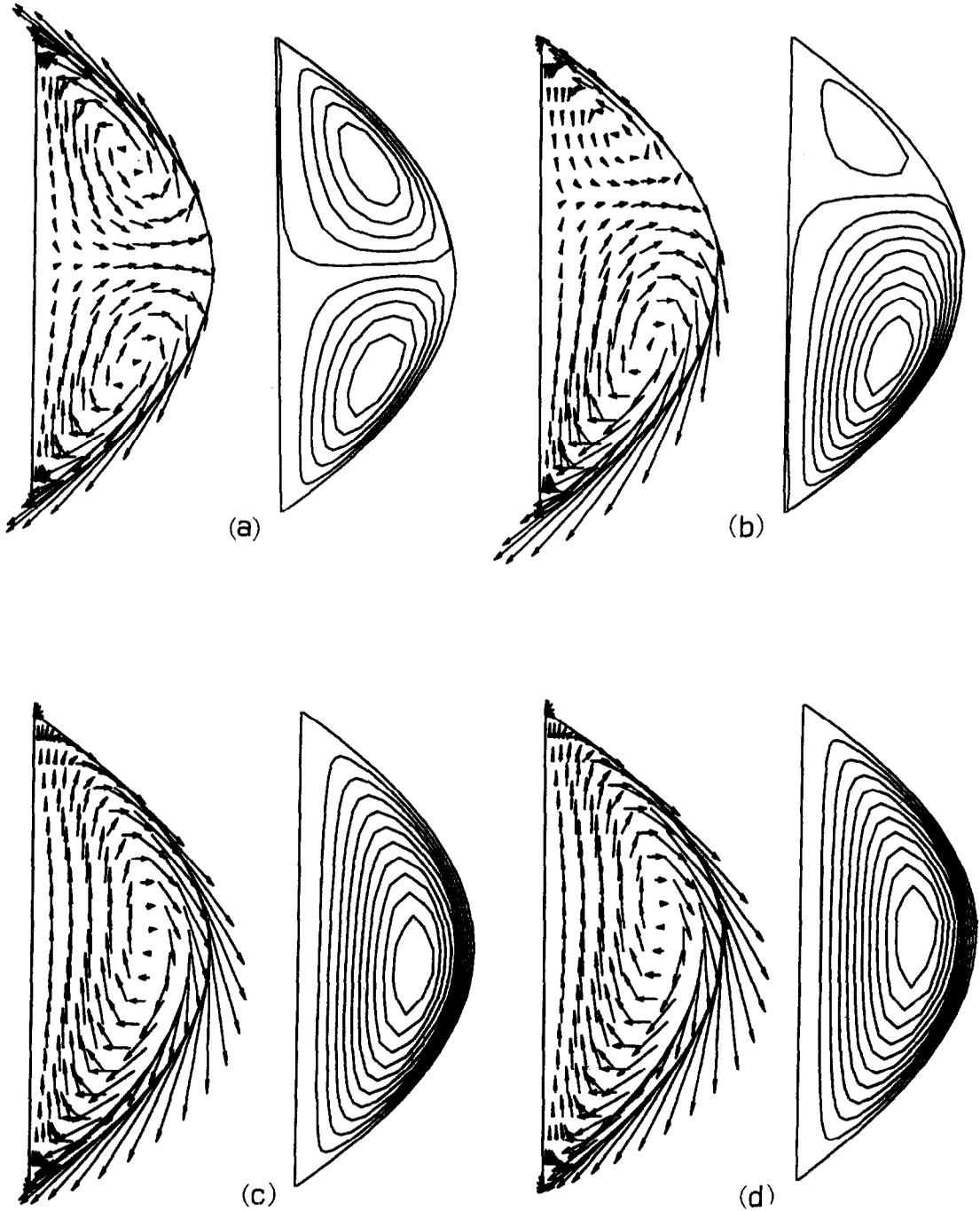
FIG. 5. Effect of external shear stress Σ. $Gr/Re_\delta = 1$, $\bar{C} = 1$, $c = 0.1$, $Q_o = 0.01$, $\gamma_T < 0$. Velocity fields and streamlines for (a) $\Sigma = 0.001$, (b) $\Sigma = 0.01$, (c) $\Sigma = 0.1$, (d) $\Sigma = 1$. Isotherms in all cases are similar to those in Fig. 2(a).

Although Everett and Haynes [15] studied the stability of static annular unduloids, it appears that no investigations have been carried out on the stability of non-stagnant fluid collars. Rayleigh's stability criterion [16] for thin, isothermal, annular films within cylinders states that films are stable to wavelengths less than $2\pi a^*$, where a^* is the radius of the film. Although it seems reasonable to expect that this limit is approximately applicable to long, thin, annular collars, it is not known how collar stability is affected by non-isothermal conditions.

4. CONCLUSIONS

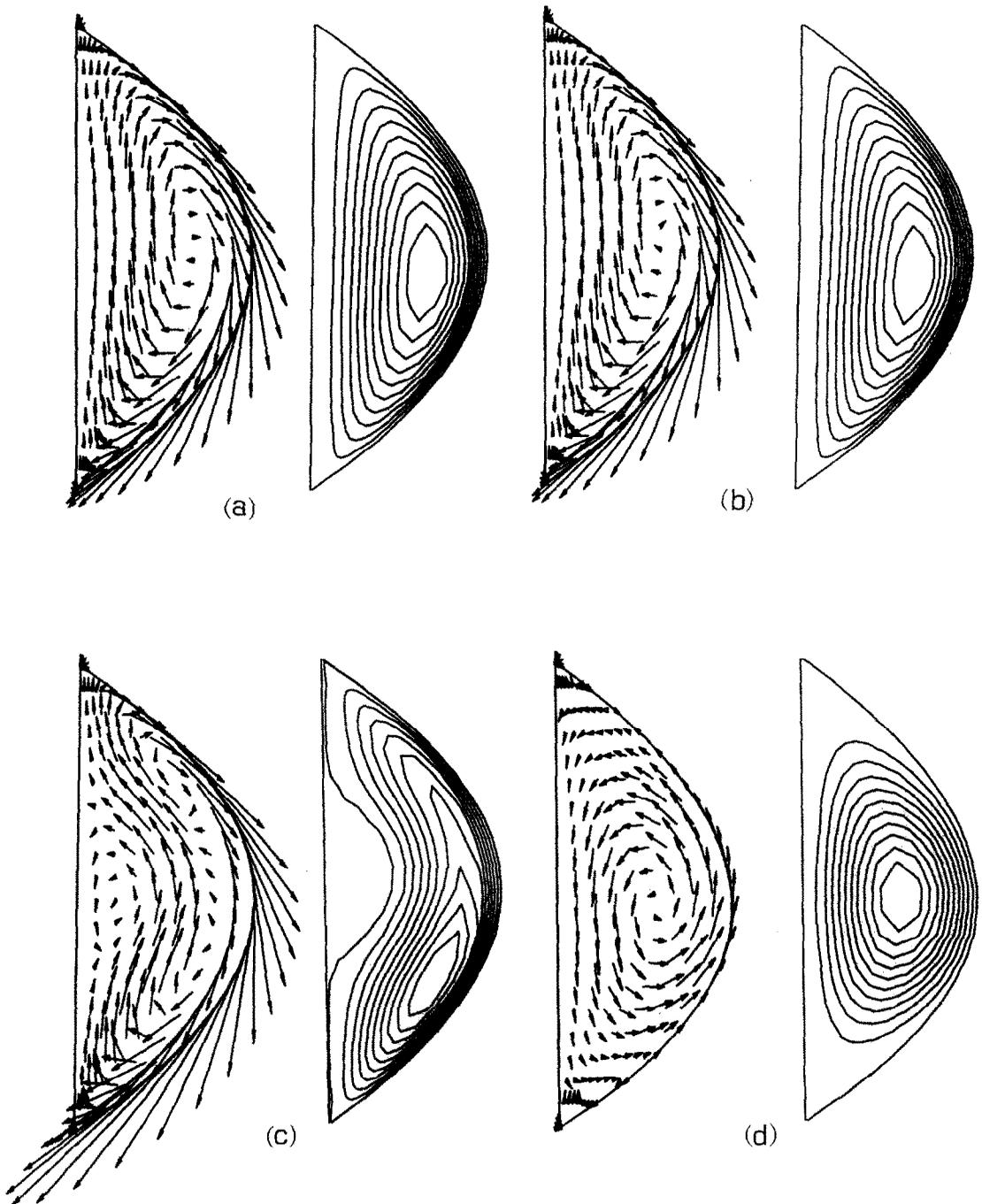The principal results of this study are summarized as follows.

FIG. 6. Effect of varying Gr/Re_δ when Σ is non-zero. $\bar{C} = 1$, $c = 0.1$, $Q_o = 0.01$, $\Sigma = 0.1$, $\gamma_\Gamma < 0$. Velocity fields and streamlines for (a) $Gr/Re_\delta = 1$, (b) $Gr/Re_\delta = 10$, (c) $Gr/Re_\delta = 100$, (d) $Gr/Re_\delta = 1000$. Isotherms in all cases are similar to those in Fig. 2(a).

1. Radial conduction through the collar constitutes the leading order heat transfer mechanism. Although fluid motion may be significant, i.e. the film Reynolds and/or Marangoni numbers may be of order one, conduction predominates due to the collar's thinness.

2. The leading order velocity field is self-similar, both along the length of the collar in the case of unicellular flow and within each cell in the case of multi-cellular flow. However, since the velocity field is also nonlinearly dependent on capillary surface shape and external heat and shear distributions, a wide range of flow behavior can arise.

3. Thermocapillary (and/or shear driven) flow occurs when GrQ/Re_δ is much smaller than $(Qh_o)'$ (and/or Σ). In this case, counter-rotating cells appear if $\Sigma + (Qh_o)' = 0$ at any point Z_i on the capillary

surface. Each pair of cells is divided by a horizontal stagnation streamline that passes into the stagnation point at $(h_o(Z_i), Z_i)$. The number of cells that appear is one greater than the number of zeros in $(\Sigma + (Qh_o)')|_{x=h_o}$ (including uni-cellular flow).

4. Buoyancy driven flow arises when GrQ/Re_δ $\Sigma + (Qh_o)'$. In this limit, uni-cellular flow exists as long as $Q(Z)$ does not change sign. However, if heat is added and removed over various portions of the capillary surface, then multi-cellular, buoyancy driven flow appears. Each resulting pair of counter-rotating cells is again separated by a horizontal stagnation streamline that passes into $(h_o(Z_i), Z_i)$ (where $Q(Z_i) = 0$). Similar to the thermocapillary regime, the number of buoyant cells appearing is one greater than the number of zeros in Q.

5. A numerical method was developed and tested in order to calculate the capillary surface shape. The method is fairly robust and could be readily applied to other 2-D capillary surface calculations.

REFERENCES

1. S. Goren, The instability of an annular thread of fluid, *J. Fluid Mech.* **12**, 309–319 (1962).
2. P. S. Hammond, Nonlinear adjustment of a thin annular film of viscous fluid surrounding a thread of another within a circular pipe, *J. Fluid Mech.* **137**, 363–384 (1983).
3. M. Johnson, R. D. Kamm, L. W. Ho, A. Shapiro and T. J. Pedley, The nonlinear growth of surface-tension-driven instabilities of a thin annular film, *J. Fluid Mech.* **233**, 141–156 (1991).
4. A. L. Yarin, A. Oron and P. Rosenau, Capillary instability of thin film on a cylinder, *Phys. Fluids A* **5**, 91–98 (1993).
5. A. Sen and S. Davis, Steady thermocapillary flows in two-dimensional slots, *J. Fluid Mech.* **121**, 163–186 (1982).
6. J.-J. Xu and S. H. Davis, Liquid bridges with thermocapillarity, *Phys. Fluids A* **26**, 2880–2886 (1983).
7. J.-J. Xu and S. H. Davis, Convective thermocapillary instabilities in liquid bridges, *Phys. Fluids A* **27**, 1102–1107 (1984).
8. A. Rybicki and J. M. Florian, Thermocapillary effects in liquid bridges. I. Thermocapillary convection, *Phys. Fluids A* **30**, 1956–1972 (1987).
9. A. Rybicki and J. M. Florian, Thermocapillary effects in liquid bridges. II. Deformation of the interface and capillary instability, *Phys. Fluids A* **30**, 1973–1983 (1987).
10. S. Ostrach, Low gravity fluid flows. In *Annual Review of Fluid Mechanics* (Edited by M. V. Van Dyke, J. V. Wehausen and J. L. Lumley), pp. 313–345. Annual Reviews, Palo Alto, CA (1982).
11. V. S. Arpaci and P. S. Larsen, *Convection Heat Transfer*, pp. 91–94. Prentice-Hall, Englewood Cliffs, NJ (1984).
12. W. Spendly, G. R. Hext and F. R. Himsworth, Sequential application of simplex designs in optimisation and evolutionary operation, *Technometrics* **4**, 441 (1962).
13. W. H. Press, B. P. Flannery, S. A. Teukolsky and W. T. Vetterling, *Numerical Recipes*, pp. 289–293. Cambridge U.P., Cambridge (1986).
14. S. R. Corriel, S. C. Hardy and M. R. Cordes, Stability of liquid zones, *J. Colloid Interface Sci.* **60**, 126–136 (1977).
15. D. H. Everett and J. M. Haynes, Model studies of capillary condensation, *J. Colloid Interface Sci.* **38**, 125 (1972).
16. Lord Rayleigh, On the stability of cylindrical fluid surfaces. In *Scientific Papers*, Vol. 3, pp. 594–596. Cambridge U.P., Cambridge (1902).